biosensors

MDPI

Article

A Paper-Based Electrochemical Sensor Based on PtNP/$COF_{TFPB-DHzDS}$@rGO for Sensitive Detection of Furazolidone

Rongfang Chen, Xia Peng, Yonghai Song and Yan Du *

National Engineering Research Center for Carbohydrate Synthesis, Key Lab of Fluorine and Silicon for Energy Materials and Chemistry of Ministry of Education, College of Chemistry and Chemical Engineering, Jiangxi Normal University, Nanchang 330022, China

* Correspondence: wjxdu01@jxnu.edu.cn or wjxdu01@163.com; Tel.: +86-0791-88120861

Abstract: Herein, a paper-based electrochemical sensor based on PtNP/$COF_{TFPB-DHzDS}$@rGO was developed for the sensitive detection of furazolidone. A cluster-like covalent organic framework ($COF_{TFPB-DHzDS}$) was successfully grown on the surface of amino-functional reduced graphene oxide (rGO-NH_2) to avoid serious self-aggregation, which was further loaded with platinum nanoparticles (PtNPs) with high catalytic activity as nanozyme to obtain PtNP/$COF_{TFPB-DHzDS}$@rGO nanocomposites. The morphology of PtNP/$COF_{TFPB-DHzDS}$@rGO nanocomposites was characterized, and the results showed that the smooth rGO surface became extremely rough after the modification of $COF_{TFPB-DHzDS}$. Meanwhile, ultra-small PtNPs with sizes of around 1 nm were precisely anchored on $COF_{TFPB-DHzDS}$ to maintain their excellent catalytic activity. The conventional electrodes were used to detect furazolidone and showed a detection limit as low as 5 nM and a linear range from 15 nM to 110 μM. In contrast, the detection limit for the paper-based electrode was 0.23 μM, and the linear range was 0.69–110 μM. The results showed that the paper-based electrode can be used to detect furazolidone. This sensor is a potential candidate for the detection of furazolidone residue in human serum and fish samples.

Keywords: paper-based electrode; reduced graphene oxide; covalent organic framework; furazolidone; electrochemical sensor

Citation: Chen, R.; Peng, X.; Song, Y.; Du, Y. A Paper-Based Electrochemical Sensor Based on PtNP/$COF_{TFPB-DHzDS}$@rGO for Sensitive Detection of Furazolidone. *Biosensors* **2022**, *12*, 904. https://doi.org/10.3390/bios12100904

Received: 7 September 2022
Accepted: 18 October 2022
Published: 21 October 2022

1. Introduction

Antibiotics are widely used in medicine and aquaculture. However, the harm caused by the use of antibiotics is irreversible. In addition, antibiotic drugs are harmful to the body's immune system, the liver, and the kidneys. The abuse of antibiotics is extraordinarily serious, and about 700,000 people die directly or indirectly every year. Furazolidone is a nitro-containing antibiotic drug, which has been widely used in aquaculture and veterinary medicine to minimize the acute effects of Escherichia coli, Shigella, Salmonella, and other infections [1–3]. Owing to the accumulation of furazolidone through the food chain, it is detrimental to the human body's immune system and even causes mutation and carcinogenesis [4,5]. Therefore, it is urgent to develop a rapid method to realize the ultrasensitive detection of furazolidone.

Covalent organic frameworks (COFs) are crystalline organic porous polymers assembled by covalent bonding of C, N, O, and other light elements, whose structure can be regulated by the periodic arrangement of organic structural units [6,7]. COFs have stable networks and open channels, which are extraordinarily conducive to the transport of electrolyte ions and have great potential in various applications. It has been reported that some COFs or COF-based sensors have better performance [8–10]. However, COFs are highly conjugated, and the π–π interaction between layers would lead to a decrease in specific surface area and poor electrical conductivity.

The development of COF composite materials to enhance electrical conductivity and specific surface area has been proven to be a feasible route. The sp^2 hybridization of reduced graphene oxide (rGO) and its extremely thin atomic thickness enable rGO to be used in many fields [11–14]. The rGO-based composites are beneficial to improve the overall conductivity of the composites. COFs can be covalently connected with rGO-NH_2 to improve the electrical conductivity of the composites. In addition, COFs are also ideal nanospacers that can reduce the stacking of adjacent rGO nanosheets and improve ion transport [15–17]. Furthermore, the presence of numerous chelating sites in the COF structure could be employed to immobilize metal nanoparticles through coordination effects. The precise anchoring of nanoparticles in the ordered holes of COFs can also avoid self-aggregation [18].

Although chromatography, immunoassay, and fluorometry exhibit high sensitivity and accuracy in the detection of antibiotic residues in water and meat products, their limitations are the complex and time-consuming sample-handling procedures, and the corresponding expensive instruments and equipment. The electrochemical method is not only simple to operate but also has high sensitivity, accuracy, and portability of equipment, which effectively overcomes the above shortcomings [19]. A paper-based analytical device was developed by Whitesides for the first time. Electrochemical paper-based analytical devices usually consist of a three-electrode setup integrated into a paper substrate, offering several benefits, such as reduced consumption of reagents and samples, portability, low cost, and availability of the raw material. They are widely used in various fields [20–24].

In this work, rGO was converted into rGO-NH_2 through amino functionalization, which was employed as the substrate material. Then, $COF_{TFPB-DHzDS}$ with abundant chelating sites were prepared through the amine-aldehyde condensation reaction of 2, 5-bis (3-(ethyl thiol) propoxy) p-benzoyl hydrazine and 1,3,5-tri(p-formylphenyl) benzene. The -NH_2 is beneficial for the $COF_{TFPB-DHzDS}$ to grow on rGO-NH_2 uniformly to form $COF_{TFPB-DHzDS}$@rGO. $COF_{TFPB-DHzDS}$ has abundant N and S atoms; therefore, Pt^{4+} can be precisely doped in its surface and internal structure through coordination and adsorption. Lastly, PtNP/$COF_{TFPB-DHzDS}$@rGO was prepared by using an in situ reduction method. The PtNP/$COF_{TFPB-DHzDS}$@rGO exposes tremendous catalytic activity. A paper-based electrochemical device based on PtNP/$COF_{TFPB-DHzDS}$@rGO composites on flexible peeled graphite paper for the detection of furazolidone was proposed. It can effectively avoid the time-consuming polishing and cleaning work of the conventional electrode, and the test results showed good performance. The device was expected to be an all-in-one electrochemical platform for the detection of antibiotics. This work provides a reference for the design and fabrication of integrated paper-based electrodes and their application in electrochemical sensing.

2. Experimental

2.1. Materials and Reagents

2,5-bis(3-(ethylthiol) propoxy) p-benzoyl hydrazine (DHzDS) and 1,3,5-tri (p-formylphenyl) benzene (TFPB) were purchased from Jilin Yanshen Technology Co., Ltd. (Beijing, China). Glacial acetic acid, anhydrous acetonitrile, tetrahydrofuran, ethanol, methanol, 1,4-dioxane, N, N-dimethylformamide, hydrochloric acid, and mesitylene were purchased from Inokay Co., Ltd. (Beijing, China) The rGO, sodium borohydride, tetranitrotetrafluoroborate diazonium salt, tetrabutylammonium tetrafluoroborate, potassium chloroplatinate, zinc powder, ammonium chloride, furazolidone, and other chemicals were purchased from Aladdin's Reagent Network (Shanghai, China). Flexible graphite paper was purchased from Jinglong Special Carbon Technology Co., Ltd. (Beijing, China). Glassy carbon electrode (GCE) was purchased from Chenhua (Beijing, China) Instrument Co., Ltd. All reagents are analytically pure and do not require further purification when used. Additionally, 0.2 M a phosphate-buffered solution was prepared from 0.2 M sodium dihydrogen phosphate and 0.2 M disodium hydrogen phosphate solution in different proportions. The ultra-pure water was purified by using a Millipore-Q System ($\rho \geq 18.2$ MΩ cm).

2.2. Instruments

Transmission electron microscopy (TEM) was performed using A JEM-2010 (HR) instrument. Scanning electron microscopy (SEM) images were collected by using a HITACHI S-3400N instrument, and the breakdown voltage was set to 15 kV. X-ray powder diffraction (XRD) analysis was performed using a D/Max 2500 V/PC instrument with Cu Kα radiation from 2° to 35° at a scanning rate of 1°/min. N_2 adsorption/desorption isotherm tests were carried out with Autosorb-iQ (Quantachrome) under 77 K. All electrochemical tests were performed at the CHI760D (Shanghai, China) Electrochemical Workstation in a conventional three-electrode system (platinum wire as an auxiliary electrode, saturated calomel (SCE) as a reference electrode, and different modified GCEs as working electrodes for routine testing, or homemade paper-based electrodes including graphite-like foam electrodes as working electrodes and counter-electrodes and Ag/AgCl as the reference electrode). Cyclic voltammetry (CVs) and differential pulse voltammetry (DPV) tests were carried out in 0.2 M static N_2 phosphate-buffered solutions. The control frequency range of electrochemical impedance (EIS) was 0.01–105 Hz, and the amplitude was 5 mV, using 5.0 mM Fe $(CN)_6^{3-/4-}$ as the signal probe. The data plotted for the calibration curve are the averages of the five experiments, and the length of the error bar indicates the magnitude of the relative deviation.

2.3. Synthesis of rGO−NH_2, $COF_{TFPB-DHzDS}$, $COF_{TFPB-DHzDS}$@rGO, and PtNP/$COF_{TFPB-DHzDS}$@rGO

Preparation of rGO-NH_2: First, 12 mg rGO was dissolved in a 10 mL anhydrous acetonitrile solution, and the solution was ultrasonic for 1 h. Then, 24 mg tetrafluoroborate diazonium salt and 329 mg tetrabutyltetrafluoroborate ammonium were added, and all the reagents were dissolved and stirred in the dark for 20 h. The solution was dried through centrifugation, and then 10 mg precipitate was added into a 40 mL ethanol–water solution (ethanol: water = 3:2). Next, 104 mg zinc powder, 2 mg ammonium chloride, and 2.3 mL glacial acetic acid were added to the solution, and the mixed solution was heated in 60 °C water bath for 3 h. After cooling down to room temperature, the rGO-NH_2 was obtained by alternate cleaning with ethanol and water and drying in a 60 °C oven.

Preparation of $COF_{TFPB-DHzDS}$: Briefly, 23 mg TFPB and 8.1 mg DHzDS were dissolved in a 3 mL mixed solution composed of mesitylene and 1,4-dioxane in a ratio of 3:1. Then, 600 μL of 6 M acetic acid was added to the solution and reacted at 120 °C for 3 days. Finally, it was cleaned 5 times with THF and dried for 6 h in a 60° coven.

Preparation of $COF_{TFPB-DHzDS}$@rGO: The steps were similar to $COF_{TFPB-DHzDS}$. Briefly, 1.62 mg TFPB and 4.6 mg DHzDS were dissolved in a 3 mL mixed solution, then 10 mg rGO-NH_2 was added, and the same concentration and volume of acetic acid solution were added after the mixture was evenly mixed. The follow-up procedure was the same as the preceding procedure.

Preparation of PtNP/$COF_{TFPB-DHzDS}$@rGO: The dried 4 mg $COF_{TFPB-DHzDS}$@rGO was dispersed into a 3 mL methanol solution, and then 2 mL 0.012 mM potassium chloride platinate solution was added and stirred at room temperature for 12 h. Next, 20 μL 0.25 M sodium borohydride solution was added, stirred for 6 h, and washed with ethanol and methylene chloride until the upper solution became colorless and transparent. Finally, the product was dried in a freeze-dryer for 4 h. The preparation process of PtNP/$COF_{TFPB-DHzDS}$@rGO materials is shown in Scheme 1.

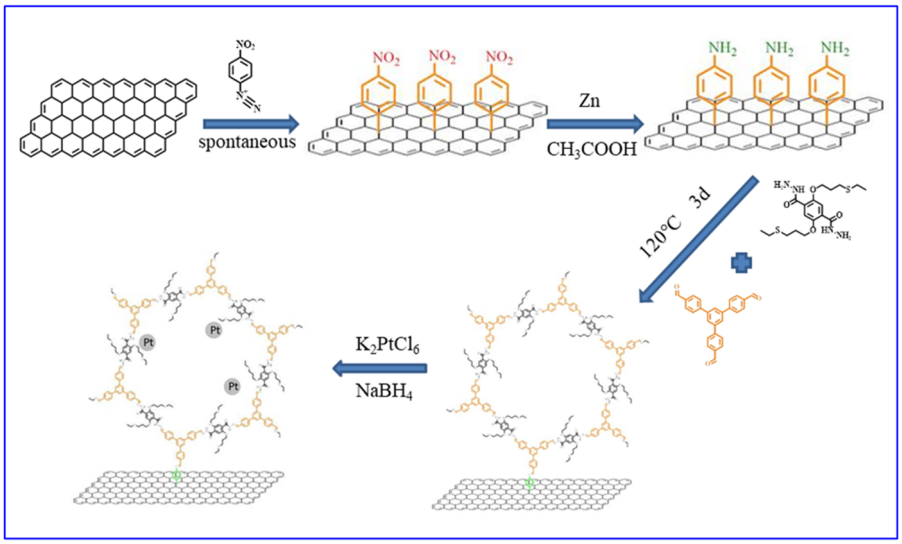

Scheme 1. Schematic illustration of the synthesis of PtNP/$COF_{TFPB-DHzDS}$@rGO.

2.4. Preparation $COF_{TFPB-DHzDS}$ and PtNP/$CO_{FTFPB-DHzDS}$@rGO/GCE

First, 2 mg $COF_{TFPB-DHzDS}$ or PtNP/$COF_{TFPB-DHzDS}$@rGO was dispersed in a 1 mL DMF solution and dissolved via sonication. Then, 10 µL suspensions were dropped onto polished GCE and dried naturally for subsequent experiments.

2.5. Preparation of Paper-Based Electrodes (ePADs)

First, the commercial carbon paper was cut into long strips of 3 mm in width and 3 cm in length by using a regular paper knife. Then, two sides of a white cardboard sheet 2 cm in width and 3 cm in length were painted with white nail polish. Next, three long carbon paper strips were pasted onto a side of the white cardboard with an interval of about 0.5 cm. The middle sections of the long carbon paper strips (about one-third of the long strips) were painted with white nail polish. The bottom sections of the long carbon paper strips were peeled off using acrylic transparent tape to obtain a new surface with graphite-like foam as electrodes (working electrode, reference electrode, and counter electrode). Then, the reference electrode was coated with a layer of conductive silver powder, and HCl was added dropwise to form AgCl/Ag. (Scheme 2).

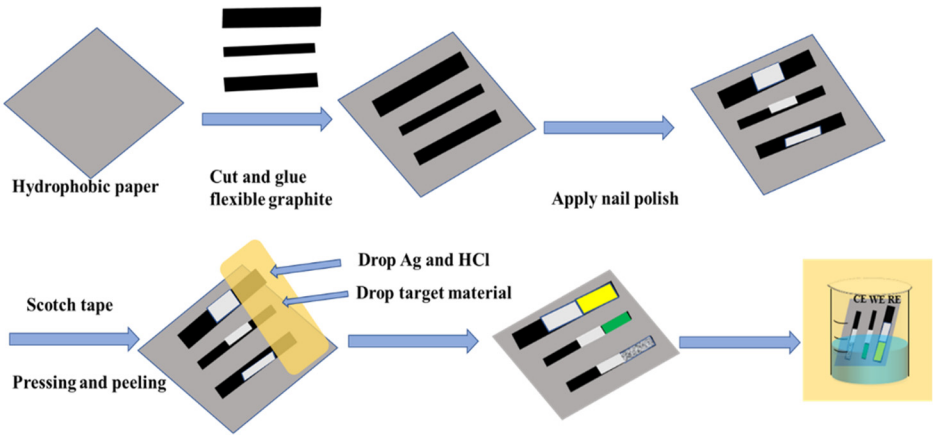

Scheme 2. Schematic illustration of the preparation of paper-based electrodes.

2.6. Preparation of PtNP/$COF_{TFPB-DHzDS}$@rGO/ePAD

The procedures were similar to PtNP/$COF_{TFPB-DHzDS}$@rGO/GCE. Briefly, 2 mg PtNP/$COF_{TFPB-DHzDS}$@ rGO was dispersed in a 1 mL DMF solution, dissolved through

sonication, then 10 μL suspensions were dropped on the lower 1/3 of the working electrodes of the paper-based electrodes. Finally, the electrode surface was dried under a tungsten lamp for 5 min.

3. Results and Discussion

3.1. Characterization of $COF_{TFPB-DHzDs}$

The SEM image (Figure S1a) showed that $COF_{TFPB-DHzDs}$ was filamentous and could stack into clusters under the interaction of the Van der Waals force. FTIR spectrum (Figure S1b) demonstrated the successful synthesis of $COF_{TFPB-DHzDs}$. The stretching vibration peak of C=N at 1620 cm^{-1} appeared in $COF_{TFPB-DHzDs}$, proving the formation of an imine bond and confirming that $COF_{TFPB-DHzDs}$ was formed through an amine-aldehyde condensation reaction between monomer TFPB and DHzDS [25]. The XRD pattern (Figure S1c) showed strong diffraction peaks at 4.77° and 26.3°, which belong to (100) and (001) crystal planes, respectively, indicating that $COF_{TFPB-DHzDs}$ has a good crystal structure [26,27]. According to the N_2 adsorption and desorption isotherms (Figure S1d) of $COF_{TFPB-DHzDs}$, the specific surface area of $COF_{TFPB-DHzDs}$ was about 153.76 m^2 g^{-1}, and the average pore size was about 1.9 nm. Its specific surface area was large, suggesting it could be used as an excellent support material [28].

3.2. Characterization of PtNP/$COF_{TFPB-DHzDS}$@rGO

The SEM (Figure 1a) and TEM (Figure 1d) images showed that rGO was a large two-dimensional slice with slight folds [29,30]. After the amino functionalization, $COF_{TFPB-DHzDS}$ could uniformly grow on the surface of rGO (Figure 1b). Compared with rGO (Figure 1a,d), the surface of $COF_{TFPB-DHzDS}$@rGO became rough. Further investigation of the surface morphology using TEM showed that the thickness of $COF_{TFPB-DHzDS}$@rGO increased, compared with the rGO, confirming the synthesis of $COF_{TFPB-DHzDS}$@rGO (Figure 1e). Figure 1c shows the SEM image of PtNP/$COF_{TFPB-DHzDS}$@rGO, whose morphology was not significantly different from that of $COF_{TFPB-DHzDS}$@rGO. Figure 1f shows that a large number of PtNPs with diameters of about 1 nm were uniformly loaded on $COF_{TFPB-DHzDS}$@ rGO (Figure S2). The formation of small PtNPs can be ascribed to the fact that Pt^{4+} uniformly adsorbed on the interlaminar structure or channel of $COF_{TFPB-DHzDS}$ during the synthesis process because $COF_{TFPB-DHzDS}$ had double chelating sites of N or S atoms [31].

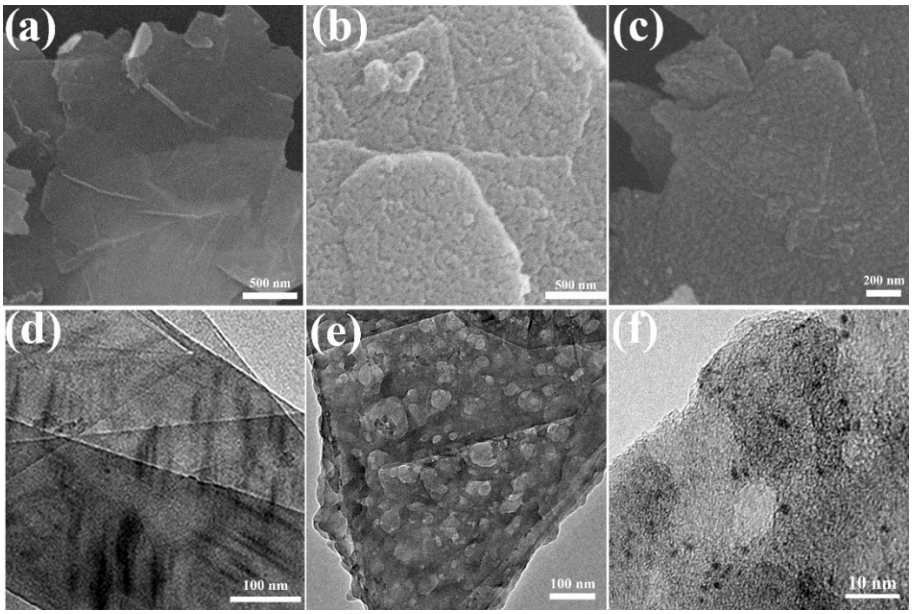

Figure 1. SEM images of (**a**) rGO, (**b**) $COF_{TFPB-DHzDS}$@rGO, and (**c**) PtNP/$COF_{TFPB-DHzDS}$@rGO. TEM images of (**d**) rGO, (**e**) $COF_{TFPB-DHzDS}$@rGO, and (**f**) PtNP/$COF_{TFPB-DHzDS}$@rGO.

The FTIR spectrum (Figure 2a) showed that rGO was basically a straight line without obvious adsorption peaks. After the amino functionalization, it could be observed that the stretching vibration peak of -NH_2 appeared in the spectrum of around 3453 cm^{-1}, which strongly proved that rGO was successfully functionalized. From the spectrum of $COF_{TFPB-DHzDS}$@rGO, it could be found that, in addition to the stretching vibration peak of -NH_2 at about 3442 cm^{-1}, there was also a vibration peak at 1630 cm^{-1}, which was attributed to C=N vibration peaks. The C=N vibration peaks were observed after the aldehyde condensation (Figure 2a), indicating that $COF_{TFPB-DHzDS}$ was grown on the surface of rGO-NH_2 successfully [32]. In the X-ray photoelectron spectrum (Figure 2b) of PtNP/$COF_{TFPB-DHzDS}$@rGO, it could be observed that the material was composed of elements such as C, N, O, and Pt. As shown in Figure 2c, 72.45 eV and 75.80 eV corresponded to the peaks of $Pt^0 4f_{7/2}$ and $Pt^0 4f_{5/2}$, respectively, which proved that the material contained PtNPs. In Figure 2d, a strong peak mainly appeared at 284.01 eV in the C 1s fine spectrum, which belonged to C−C or C=C, while the three strong peaks appearing at 397.98 eV, 399.06 eV, and 399.88 eV in Figure 3e corresponded to =NH, −NH− and −N=N−, respectively [33–35]. In the XPS fine spectrum of O 1s (Figure 2f), the peak at 530.70 eV corresponded to C−O, while the peak at 532.60 eV corresponded to C=O. In summary, taking advantage of the large specific surface area and good electrical conductivity of rGO, and the porous framework structure and double chelation sites of $COF_{TFPB-DHzDS}$, Pt^{4+} was in situ reduced through a chemical reduction method, and a large amount of small-sized PtNPs were uniformly loaded on $COF_{TFPB-DHzDS}$@rGO. This work provides a new reference for the construction of composite materials.

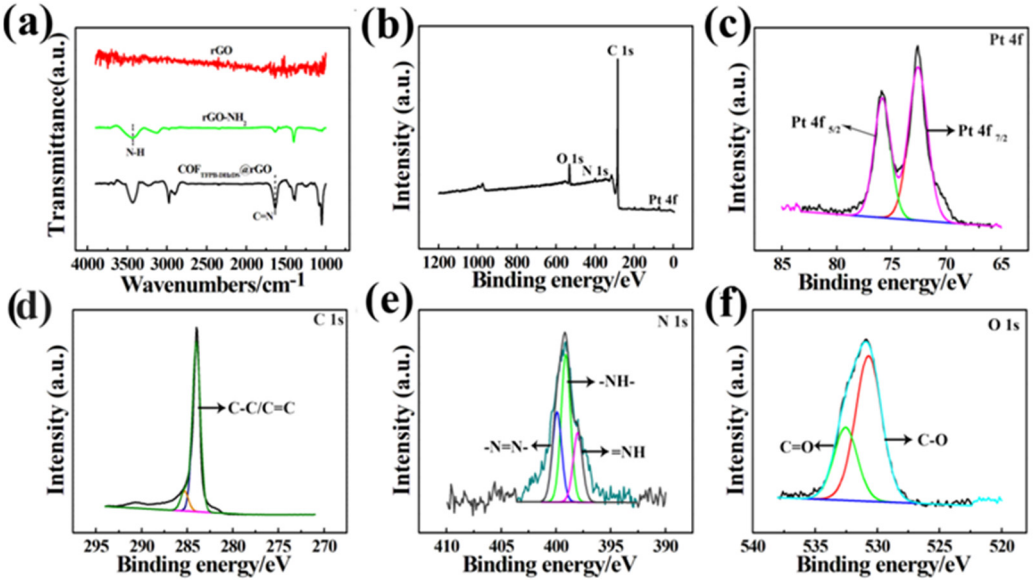

Figure 2. (**a**) FTIR spectra of rGO, rGO-NH_2, and $COF_{TFPB-DHzDS}$@rGO; (**b**) XPS spectrum of PtNP/$COF_{TFPB-DHzDS}$@rGO; (**c**–**f**) fine XPS spectra of Pt 4f, C 1s, N 1s, and O 1s, respectively.

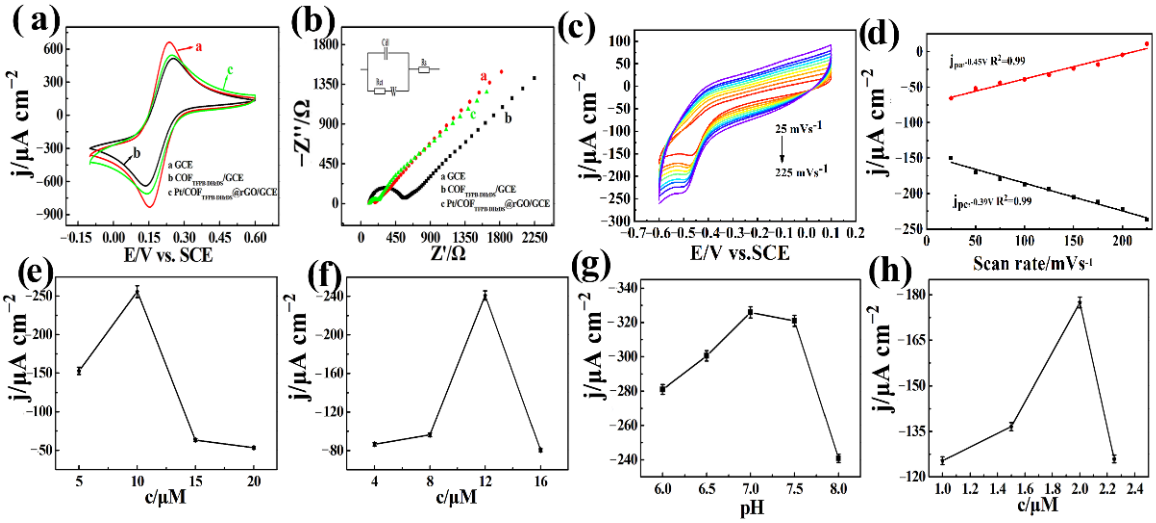

Figure 3. (**a**) CVs curves and (**b**) EIS diagram (inset is equivalent circuit diagram) of bare GCE (curve a), $COF_{TFPB-DHzDS}$/GCE (curve b), and PtNP/$COF_{TFPB-DHzDS}$@rGO/GCE (curve c) in 0.1 M KCl solution containing 5 mM $[Fe(CN)_6]^{3-/4-}$; (**c**) CVs of PtNP/$COF_{TFPB-DHzDS}$@rGO/GCE at different scan rates (25 mV s^{-1} to 225 mV s^{-1}) in 0.1 M N_2-statured phosphate-buffered solution (pH = 7.0) with 10 μM furazolidone; (**d**) the corresponding fitting curves between current density and scan rates; (**e**) the plots of peak current density versus different concentrations of TFPB, (**f**) different concentrations of potassium chloroplatinate, (**g**) different pH levels, and (**h**) different concentrations of PtNP/$COF_{TFPB-DHzDS}$@rGO.

3.3. Electrochemical Behaviors of PtNP/$COF_{TFPB-DHzDS}$@rGO/GCE

Figure 3a shows the CV curves of GCE, $COF_{TFPB-DHzDS}$/GCE, and PtNP/$COF_{TFPB-DHzDS}$@rGO/GCE in a 0.1 M KCl solution containing 5 mM $[Fe(CN)_6]^{3-/4-}$. The bare GCE had a pair of reversible redox peaks with a peak-to-peak potential difference (ΔEp) of 85 mV. After the modification with $COF_{TFPB-DHzDS}$, the peak current was obviously reduced, and ΔEp was increased to 118 mV, indicating that $COF_{TFPB-DHzDS}$ inhibited the electron transfer. The PtNP/$COF_{TFPB-DHzDS}$@rGO-modified electrode had a larger peak current and smaller ΔEp (about 98 mV). This suggested that PtNPs and rGO enhanced the reversibility of the reaction and significantly improved its electrochemical performance. This result is mainly attributed to the excellent electrical conductivity of rGO and PtNPs. Figure 3b shows the EIS of COF (curve a), $COF_{TFPB-DHzDS}$@rGO (curve b), and PtNP/$COF_{TFPB-DHzDS}$@rGO. The results indicated that PtNP/$COF_{TFPB-DHzDS}$@rGO has the smallest charge transfer resistance, similar to GCE. The CVs of PtNP/$COF_{TFPB-DHzDS}$@rGO/GCE in a 0.1 M N_2-statured phosphate-buffered solution (pH = 7.0) with 10 μM furazolidone showed an obvious reduction of furazolidone and an indistinct oxidation peak. According to a previous report [36], the redox mechanism is speculated to be that the nitrogroup contained in the structure of furazolidone is reduced under the synergistic catalysis of Pt and rGO. With the increase in the scanning rate, the peak current density of furazolidone increased (Figure 3c), and a good linear relationship was presented (Figure 3d), indicating that the reaction process was a typical surface control process [37,38].

3.4. Optimization of the Experimental Conditions

The amount of $COF_{TFPB-DHzDS}$ growing on the rGO surface, the amount of PtNPs immobilized on $COF_{TFPB-DHzDS}$@rGO, the pH value of electrolyte solution, and the concentration of PtNP/$COF_{TFPB-DHzDS}$@rGO dispersion had significant effects on the performance of the constructed electrochemical sensor, and accordingly, these conditions were optimized in order to realize the sensitive detection of furazolidone (Figure 3e–h).

Figure 3e indicates that with the amount of $COF_{TFPB-DHzDS}$ on rGO, the current responses gradually increased. When the amount exceeded 10 μM, the current responses decreased because $COF_{TFPB-DHzDS}$ seriously accumulated. The amount of $COF_{TFPB-DHzDS}$@rGO

was maintained at 3 mg, and the current response of PtNP/$COF_{TFPB-DHzDS}$@rGO prepared at different concentrations of potassium chloroplatinate to furazolidone was investigated. It could be seen intuitively from Figure 3f that, when the concentration of potassium chloroplatinate was 12 μM, the resulting sensor had the optimum current response to furazolidone. When the concentration of potassium chloroplatinate was further increased to 16 μM, the peak current density of furazolidone decreased instead. The reason might be that the ion concentration was too high, thus leading to the larger size of the formed PtNPs with decreased catalytic ability. The detection of furazolidone in a 0.2 M phosphate-buffered solution with different pH levels by using PtNP/$COF_{TFPB-DHzDS}$@rGO/GCE was studied, and the results are shown in Figure 3g. It could be seen that the peak current density value reached the maximum at pH = 7.0. Therefore, a phosphate-buffered solution with pH = 7.0 was used as the optimal electrolyte solution for the detection of furazolidone by using PtNP/$COF_{TFPB-DHzDS}$@rGO/GCE. Finally, the amount of PtNP/$COF_{TFPB-DHzDS}$@rGO modified on GCE was optimized, and the results are shown in Figure 3h. As the concentration of PtNP/$COF_{TFPB-DHzDS}$@rGO increased, the catalytic current of furazolidone gradually increased and reached the maximum value at 2 mg mL^{-1}. When the concentration of PtNP/$COF_{TFPB-DHzDS}$@rGO exceeded 2 mg mL^{-1}, the PtNP/$COF_{TFPB-DHzDS}$@rGO accumulated on the surface of GCE, and the modified layer became thicker, which hindered the mass transfer, resulting in a decrease in the peak current density value. Therefore, 2 mg mL^{-1} of PtNP/$COF_{TFPB-DHzDS}$@rGO was selected as the optimal modification concentration.

3.5. Electrochemical Sensors Based on PtNP/$COF_{TFPB-DHzDS}$@rGO for Furazolidone

The DPV curves of GCE, $COF_{TFPB-DHzDS}$/GCE, and PtNP/$COF_{TFPB-DHzDS}$@rGO/GCE in a 0.2 M N_2-saturated phosphate-buffered solution (pH = 7.0) with 30 μM furazolidone showed that the PtNP/$COF_{TFPB-DHzDS}$@rGO/GCE exhibited excellent furazolidone reduction performance with a large reduction peak current and a positive reduction potential, thus providing a sensitive method for furazolidone determination (Figure 4a). The highly sensitive response of PtNP/$COF_{TFPB-DHzDS}$@rGO/GCE to furazolidone was attributed to the high catalytic activity of PtNP/$COF_{TFPB-DHzDS}$@rGO and the strong interaction between the PtNP/$COF_{TFPB-DHzDS}$@rGO and furazolidone [39,40]. The high electrical conductivity of PtNP/$COF_{TFPB-DHzDS}$@rGO accelerated the electron transfer to furazolidone during the redox process, and the rich aromatic system in $COF_{TFPB-DHzDS}$ facilitated π–π stacking interactions with conjugated molecules such as furazolidone. Furthermore, the large surface area of the PtNP/$COF_{TFPB-DHzDS}$@rGO provided abundant sites for analyte binding and reduction. PtNPs as nanozymes catalyzed the reduction of furazolidone, and rGO was beneficial to improve the conductivity. Under the synergistic effect, the peak current became larger. Due to the existence of PtNPs, the overpotential of the reaction was reduced, making furazolidone easier to reduce, so the more positive the potential was, the more the peak potential shifted to the right.

Next, the current responses of PtNP/$COF_{TFPB-DHzDS}$@rGO/GCE in furazolidone solutions with different concentrations were measured. Figure 4b shows the response of DPV to furazolidone with different concentrations. The results showed that the peak current response increased as the concentration of furazolidone increased, which maintained a linear relationship over a wide range (15.0 nM−110 μM). Figure 4c shows the corresponding linear relationship between the peak current density and the concentration of furazolidone. Each value was the average of the resulting values that were repeated five times. The linear equation was $j = -84.6511c - 3.2922$ ($R^2 = 0.99$), where j and c were the peak current density and the concentration of furazolidone solution, respectively. The detection limit of PtNP/$COF_{TFPB-DHzDS}$@rGO/GCE for furazolidone was 5.0 nM.

Compared with other electrochemical sensors, this sensor also had some advantages (as shown in Table 1) [41–49]. Compared with $NiCo_2O_4$@C/GCE and NST/GCE, PtNP/$COF_{TFPB-DHzDS}$@rGO/GCE had a lower detection limit, while compared with NST/GCE and rGO/GCE, the constructed furazolidone sensor had a wider detection range. Then, the selectivity of PtNP/$COF_{TFPB-DHzDS}$@rGO/GCE was tested. As shown in

Figure 4d, the PtNP/$COF_{TFPB-DHzDS}$@rGO/GCE showed good selectivity in the presence of potentially interfering substances. The repeatability and stability of PtNP/$COF_{TFPB-DHzDS}$@rGO/GCE were also investigated. Six different PtNP/$COF_{TFPB-DHzDS}$@rGO/GCE electrodes were prepared and used to detect 100 μM furazolidone with a relative standard deviation of 0.93%, which proved that the prepared sensor had good repeatability (Figure 4e). Subsequently, the same PtNP/$COF_{TFPB-DHzDS}$@rGO/GCE was tested seven times after different storing times, and the current signal only decreased by 11.80% after 30 days, indicating that PtNP/$COF_{TFPB-DHzDS}$@rGO/GCE also had good stability (Figure 4f).

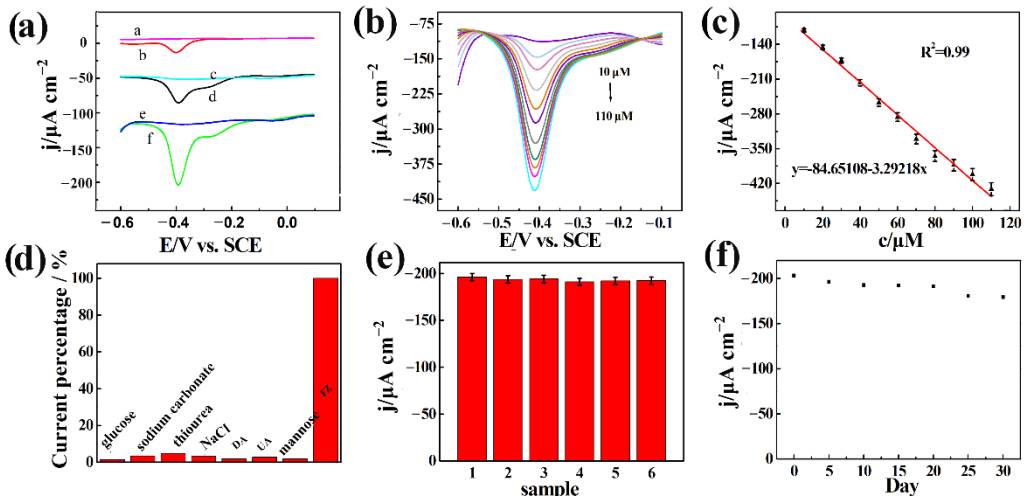

Figure 4. (**a**) DPV diagram of GCE (curves a and b), $COF_{TFPB-DHzDS}$/GCE (curves c and d), and PtNP/$COF_{TFPB-DHzDS}$@rGO/GCE (curves e and f) before (**a**,**c**,**e**) and after (**b**,**d**,**f**) the addition of furazolidone in N_2-saturated 0.2 M phosphate-buffered solution (pH = 7); (**b**) DPV of PtNP/$COF_{TFPB-DHzDS}$@rGO/GCE in N_2-saturated 0.2 M phosphate-buffered solution (pH = 7) in the presence of furazolidone with different concentration; (**c**) the linear curve of the corresponding peak current density and concentration; (**d**) histogram of PtNP/$COF_{TFPB-DHzDS}$@rGO/GCE for different interfering substances (glucose, sodium carbonate, thiourea, NaCl, UA, DA, mannose); (**e**) current responses of six different PtNP/$COF_{TFPB-DHzDS}$@rGO/GCE to 100 μM furazolidone; (**f**) current responses of PtNP/$COF_{TFPB-DHzDS}$@rGO/GCE to 100 μM furazolidone after different days.

Table 1. Comparison of different kinds of furazolidone sensors.

Electrode	LOD (μM)	Linear Range (μM)	References
$NiCo_2O_4$@C/GCE	7.05×10^{-3}	0.5–300	[41]
NGDYQD/GCE	0.0126	0.14–400	[42]
RGO/GCE	0.3×10^{-3}	2–10.0	[43]
MoN@S−GCN/GCE	6.9×10^{-3}	0.5–2405	[44]
NH−MnO_2−NAuF−FTO	6.6×10^{-3}	0.01–10	[45]
Pt−Re NP/PAC	0.75	0.2–117.7	[46]
MWCNT/GCE	2.3	3–800	[47]
CeW/GO/GCE	5.4×10^{-3}	1–120	[48]
COF@NH_2−CNT/GCE	7.5×10^{-3}	0.2–100	[49]
PtNP/$COF_{TFPB-DHzDS}$@rGO/ePAD	0.23	0.69–100	This work
PtNP/$COF_{TFPB-DHzDS}$@rGO/GCE	5×10^{-3}	0.015–110	This work

Figure 5a,b shows the CV and EIS curves of ePAD and PtNP/$COF_{TFPB-DHzDS}$@rGO/ePAD in a 0.1 M KCl solution containing 5 mM $[Fe(CN)_6]^{3-/4-}$. The bare ePAD had a pair of reversible redox peaks. After the modification of the target material, the peak current slightly decreased, and the impedance slightly increased. These experimental results were similar to those of GCE, which proved that the paper-based electrode was successfully prepared.

The current responses of PtNP/$COF_{TFPB-DHzDS}$@rGO/ePAD in furazolidone solutions with different concentrations were measured. Figure 5b shows the response of the paper-based electrochemical sensor to the different concentrations of furazolidone. The results showed that the peak current response increased as the concentration of furazolidone increased, which maintained a linear relationship over a wide range (0.69 μM −100 μM). Figure 5c shows a linear relationship between the peak current density and the concentration of furazolidone. The linear equation was j = –14.24c–2170.91 (R^2 = 0.99), where j and c are the peak current density and the concentration of furazolidone solution, respectively. The detection limit of the paper-based electrochemical sensor was 0.23 μM. The paper-based electrodes had good linear ranges, which proved that the preparation of paper-based electrodes was successful.

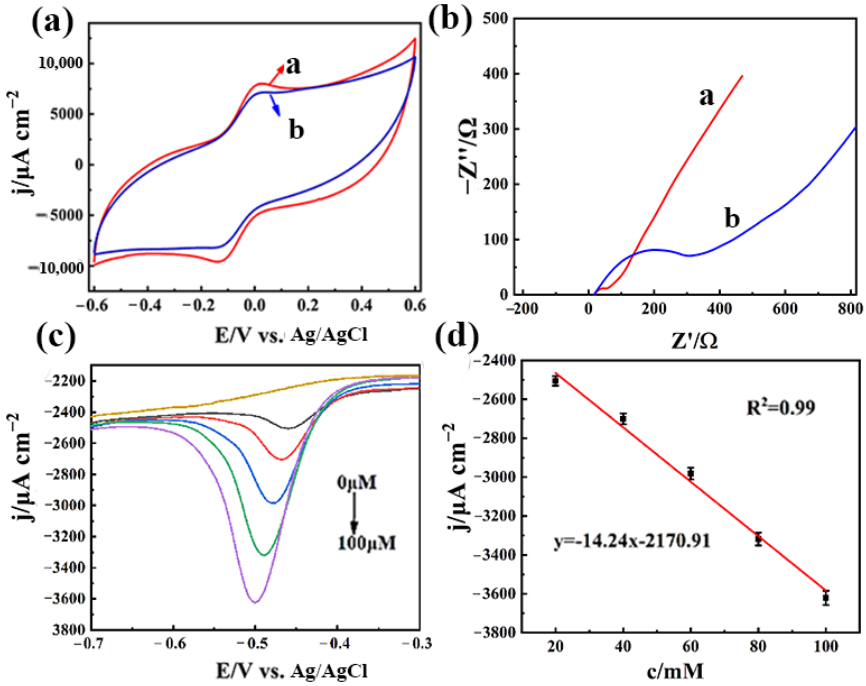

Figure 5. (**a**) CVs curves and (**b**) EIS diagram of ePAD (curve a) and PtNP/$COF_{TFPB-DHzDS}$@rGO/ePAD (curve b) in 0.1 M KCl solution containing 5 mM $[Fe(CN)_6]^{3-/4-}$; (**c**) DPV of furazolidone with different concentrations detected by PtNP/$COF_{TFPB-DHzDS}$@rGO/ePAD; (**d**) linear curves corresponding to peak current density and concentration of PtNP/$COF_{TFPB-DHzDs}$@rGO/ePAD.

3.6. Determination of Furazolidone in Human Serum and Fish Sample

The diluted human serum was used as actual samples, and the results showed that the paper-based electrode sensor had a good recovery rate, which proved that the PtNP/$COF_{TFPB-DHzDS}$@rGO/ePAD sensor has the potential to detect furazolidone in real examples (Table S1). In addition, fish were raised for three days and given different amounts of furazolidone in the water (Figure S3). The water in the tank was used for the actual sample testing, and the results are shown in Table S2, which indicates that a part of furazolidone was absorbed by the fish.

4. Conclusions

In conclusion, an electrochemical sensing platform based on a homemade paper-based electrode loaded with PtNP/$COF_{TFPB-DHzDS}$@rGO composite was developed to detect furazolidone. The rGO−NH_2 was used to guide the growth of $COF_{TFPB-DHzDS}$ on its surface to prepare $COF_{TFPB-DHzDS}$@rGO composites in which $COF_{TFPB-DHzDS}$ were covalently linked on rGO−NH_2. Then, Pt^{4+} was first coordinated with the N and S atoms of $COF_{TFPB-DHzDS}$, and subsequently, PtNP/$COF_{TFPB-DHzDS}$@rGO was obtained by reducing Pt^{4+}. $COF_{TFPB-DHzDS}$ was uniformly distributed on the layered rGO, and the

ultra-small PtNPs were formed on $COF_{TFPB-DHzDS}$@rGO as nanozymes. The rGO and PtNPs increased the electrical conductivity of $COF_{TFPB-DHzDS}$, and the catalytic activity of PtNP/$COF_{TFPB-DHzDS}$@rGO was enhanced. Therefore, the proposed furazolidone electrochemical sensor based on PtNP/$COF_{TFPB-DHzDS}$@rGO nanocomposites had a low detection limit (5 nM), a wide determination range (15 nM−110 μM) based on GCE, and good repeatability and stability. In contrast, the limit of detection for the paper-based electrode was 0.23 μM and the linear range was 0.69–100 μM. In addition, this work provides a reference for the covalent attachment of COFS materials on the surface of rGO and the synthesis of ultra-small-sized nanoparticles.

Supplementary Materials: The following supporting information can be downloaded at: https://www.mdpi.com/article/10.3390/bios12100904/s1. Figure S1. SEM image (a), FTIR spectrum (b), XRD pattern (c) and N2 adsorption/desorption iso-therm (d) of COFTFPB− DHzDS. Figure S2. the particle size distribution of PtNPs in PtNPs/COFTFPB−DHzDS@rGO. Figure S3. Picture of fish with furazolidone. Table S1. The determination of furazolidone in human serum sample by PtNPs/COFTFPB−DHzDS@ rGO/PBE. Table S2. The determination of furazolidone in fish sample by PtNPs/COFTFPB−DHzDS@rGO/PBE.

Author Contributions: R.C. and Y.D. conceived and planned the study. R.C. and X.P. carried out the experiments. R.C., Y.S. and X.P. reviewed and edited the manuscript. Y.D. was responsible for the supervision, project administration, and funding acquisition. All authors provided critical feedback and helped shape the research and analysis. All authors have read and agreed to the published version of the manuscript.

Funding: This work was financially supported by the National Natural Science Foundation of China (21964010).

Institutional Review Board Statement: All experiments involving animals were in accordance with the guidelines of the National Institute of Food and Drug, Nanchang, China, and approved by the Institutional Ethical Committee (IEC) of Jiangxi University of Traditional Chinese Medicine. This article does not contain any studies with human participants performed by any of the authors.

Informed Consent Statement: Not applicable.

Data Availability Statement: The data are available under the request to the correspondence.

Conflicts of Interest: The authors declare no conflict of interest.

References

1. Liu, S.; Dou, L.; Yao, X.; Zhang, W.; Zhao, B.; Wang, Z.; Ji, Y.; Sun, J.; Xu, B.; Zhang, D.; et al. Polydopamine nanospheres as high-affinity signal tag towards lateral flow immunoassay for sensitive furazolidone detection. *Food Chem.* **2020**, *315*, 126310. [CrossRef] [PubMed]
2. Feitosa, I.; Mori, B.; Santos, A.; Villanova, J.; Teles, C.; Costa, A. What are the immunopharmacological effects of furazolidone? A systematic review. *Immunopharm. Immunot.* **2021**, *43*, 674–679. [CrossRef] [PubMed]
3. Rajakumaran, R.; Anupriya, J.; Chen, S.-M. 2D-Titanium carbide MXene/RGO composite modified electrode for selective detection of carcinogenic residue furazolidone in food and biological samples. *Mater. Lett.* **2021**, *297*, 129979. [CrossRef]
4. Su, L.; Wang, L.; Yao, X.; Yin, X.; Zhang, H.; Zhao, M.; Liu, S.; Wang, Z.; Wang, J.; Zhang, D. Small size nanoparticles-Co_3O_4 based lateral flow immunoassay biosensor for highly sensitive and rapid detection of furazolidone. *Talanta* **2020**, *211*, 120729. [CrossRef]
5. Sun, Y.; Waterhouse, G.; Xu, L.; Qiao, X.; Xu, Z. Three-dimensional electrochemical sensor with covalent organic framework decorated carbon nanotubes signal amplification for the detection of furazolidone. *Sen. Actuators B* **2020**, *321*, 128501. [CrossRef]
6. Xu, J.; Dou, L.; Liu, S.; Su, L.; Yin, X.; Ren, J.; Hu, H.; Zhang, D.; Sun, J.; Wang, Z.; et al. Lateral flow immunoassay for furazolidone point-of-care testing: Cater to the call of saving time, labor, and cost by coomassie brilliant blue labeling. *Food Chem.* **2021**, *352*, 129415. [CrossRef]
7. Meng, Y.; Luo, Y.; Shi, J.; Ding, H.; Lang, X.; Chen, W.; Zheng, A.; Sun, J.; Wang, C. 2D and 3D porphyrinic covalent organic frameworks: The influence of dimensionality on functionality. *Angew. Chem. Int. Ed.* **2020**, *59*, 3624–3629. [CrossRef] [PubMed]
8. Chen, J.Q.; Zheng, Q.Q.; Xiao, S.J.; Zhang, L.; Liang, R.P.; Ouyang, G.; Qiu, J.D. Construction of two-dimensional fluorescent covalent organic framework nanosheets for the detection and removal of nitrophenols. *Anal. Chem.* **2022**, *94*, 2517–2526. [CrossRef] [PubMed]

9. Wu, N.; Wang, L.; Xie, Y.; Du, Y.; Song, Y.; Wang, L. Double signal ratiometric electrochemical riboflavin sensor based on macroporous carbon/electroactive thionine-contained covalent organic framework. *J. Colloid Interface Sci.* **2022**, *608*, 219–226. [CrossRef]
10. Wang, X.; Yang, S.; Shan, J.; Bai, X. Novel electrochemical acetylcholinesterase biosensor based on core-shell covalent organic framework@multi-walled carbon nanotubes (COF@MWCNTs) composite for detection of malathion. *Int. J. Electrochem. Sci.* **2022**, *17*, 220543. [CrossRef]
11. Taniselass, S.; Arshad, M.K.M.; Gopinath, S.C.B. Graphene-based electrochemical biosensors for monitoring noncommunicable disease biomarkers. *Biosens. Bioelectron.* **2019**, *130*, 276–292. [CrossRef] [PubMed]
12. Tarcan, R.; Todor-Boer, O.; Petrovai, I.; Leordean, C.; Astilean, S.; Botiz, I. Reduced graphene oxide today. *J. Mater. Chem. C* **2020**, *8*, 1198–1224. [CrossRef]
13. Itsoponpan, T.; Thanachayanont, C.; Hasin, P. Sponge-like $CuInS_2$ microspheres on reduced graphene oxide as an electrocatalyst to construct an immobilized acetylcholinesterase electrochemical biosensor for chlorpyrifos detection in vegetables. *Sens. Actuators B* **2021**, *337*, 129775. [CrossRef]
14. Kudr, J.; Zhao, L.; Nguyen, E.P.; Arola, H.; Nevanen, T.K.; Adam, V.; Zitka, O.; Merkoci, A. Inkjet-printed electrochemically reduced graphene oxide microelectrode as a platform for HT-2 mycotoxin immunoenzymatic biosensing. *Biosens. Bioelectron.* **2020**, *156*, 112109. [CrossRef] [PubMed]
15. Li, Y.; Yuan, S.; Xia, Y.; Zhao, W.; Easton, C.D.; Selomulya, C.; Zhang, X. Mild annealing reduced graphene oxide membrane for nanofiltration. *J. Membr. Sci.* **2020**, *601*, 117900. [CrossRef]
16. Li, Z.; Wu, D.; Ouyang, Y.; Wu, H.; Jiang, M.; Wang, F.; Zhang, L.Y. Synthesis of hollow cobalt phosphide nanocrystals with ultrathin shells anchored on reduced graphene oxide as an electrocatalyst toward hydrogen evolution. *Appl. Surf. Sci.* **2020**, *506*, 144975. [CrossRef]
17. Liu, B.; Xiao, B.; Cui, L. Electrochemical analysis of carbaryl in fruit samples on graphene oxide-ionic liquid composite modified electrode. *J. Food Compos. Anal.* **2015**, *40*, 14–18. [CrossRef]
18. Liu, Y.; Ma, Y.; Zhao, Y.; Sun, X.; Gandara, F.; Furukawa, H.; Liu, Z.; Zhu, H.; Zhu, C.; Suenaga, K.; et al. Weaving of organic threads into a crystalline covalent organic framework. *Science* **2016**, *351*, 365–369. [CrossRef]
19. Zamarchi, F.; Silva, T.; Winiarsk, J.; Santana, E.; Vieira, I. Polyethylenimine-based electrochemical sensor for the determination of caffeic acid in aromatic herbs. *Chemosensors* **2022**, *10*, 375. [CrossRef]
20. Liu, X.; Gao, X.; Yang, L.; Zhao, Y.; Li, F. Metal-organic framework-functionalized paper-based electrochemical biosensor for ultrasensitive exosome assay. *Anal. Chem.* **2021**, *93*, 11792–11799. [CrossRef]
21. Pesaran, S.; Rafatmah, E.; Hemmateenejad, B. An all-in-one solid state thin-layer potentiometric sensor and biosensor based on three-dimensional origami paper microfluidics. *Biosensors* **2021**, *11*, 44. [CrossRef] [PubMed]
22. Sanchez-Calvo, A.; Blanco-Lopez, M.C.; Costa-Garcia, A. Paper-based working electrodes coated with mercury or bismuth films for heavy metals determination. *Biosensors* **2020**, *10*, 52. [CrossRef]
23. Huang, Y.; Song, Y.; Gou, L.; Zou, Y. A Novel Wearable Flexible Dry Electrode Based on Cowhide for ECG Measurement. *Biosensors* **2021**, *11*, 44. [CrossRef] [PubMed]
24. Pereira, F.; Santana, R.; Spinelli, A. Electrochemical paper-based analytical devices containing magnetite nanoparticles for the determination of vitamins B_2 and B_6. *Microchem. J.* **2022**, *179*, 107588. [CrossRef]
25. Liang, H.; Wang, L.; Yang, Y.; Song, Y.; Wang, L. A novel biosensor based on multienzyme microcapsules constructed from covalent-organic framework. *Biosens. Bioelectron.* **2021**, *193*, 113553. [CrossRef] [PubMed]
26. Wang, H.; Wang, H.; Wang, Z.; Tang, L.; Zeng, G.; Xu, P.; Chen, M.; Xiong, T.; Zhou, C.; Li, X.; et al. Covalent organic framework photocatalysts: Structures and applications. *Chem. Soc. Rev.* **2020**, *49*, 4135–4165. [CrossRef]
27. Yang, Y.; Tang, X.; Wu, J.; Dong, Z.; Yan, Y.; Zheng, S.; Fan, J.; Li, X.; Cai, S.; Zhang, W. Transformation of a hydrazone-linked covalent organic framework into a highly stable hydrazide-linked one. *ACS Appl. Polym. Mater.* **2022**, *4*, 4624–4631. [CrossRef]
28. Liang, H.; Xu, M.; Zhu, Y.; Wang, L.; Xie, Y.; Song, Y.; Wang, L. H_2O_2 ratiometric electrochemical sensors based on nanospheres derived from ferrocence-modified covalent organic frameworks. *ACS Appl. Nano Mater.* **2019**, *3*, 555–562. [CrossRef]
29. da Silva, M.; Vanzela, H.; Defavari, L.; Cesarino, I. Determination of carbamate pesticide in food using a biosensor based on reduced graphene oxide and acetylcholinesterase enzyme. *Sens. Actuators B.* **2018**, *277*, 555–561. [CrossRef]
30. Torul, H.; Yarali, E.; Eksin, E.; Ganguly, A.; Benson, J.; Tamer, U.; Papakonstantinou, P.; Erdem, A. Paper-based electrochemical biosensors for voltammetric detection of miRNA biomarkers using reduced graphene oxide or MoS_2 nanosheets decorated with gold nanoparticle electrodes. *Biosensors* **2021**, *11*, 101. [CrossRef] [PubMed]
31. Park, E.; Jack, J.; Hu, Y.; Wan, S.; Huang, S.; Jin, Y.; Maness, P.; Yazdi, S.; Ren, Z.; Zhang, W. Covalent organic framework-supported platinum nanoparticles as efficient electrocatalysts for water reduction. *Nanoscale* **2020**, *12*, 2596–2602. [CrossRef] [PubMed]
32. Zhang, P.; Sun, T.; Rong, S.; Zeng, D.; Yu, H.; Zhang, Z.; Chang, D.; Pan, H. A sensitive amperometric AChE-biosensor for organophosphate pesticides detection based on conjugated polymer and Ag-rGO-NH_2 nanocomposite. *Bioelectrochemistry* **2019**, *127*, 163–170. [CrossRef]
33. Han, J.; Yu, J.; Guo, Y.; Wang, L.; Song, Y. COF_{BTLP-1}/three-dimensional macroporous carbon electrode for simultaneous electrochemical detection of Cd^{2+}, Pb^{2+}, Cu^{2+} and Hg^{2+}. *Sen. Actuators B* **2020**, *321*, 128498. [CrossRef]
34. Wang, L.; Xie, Y.; Yang, Y.; Liang, H.; Wang, L.; Song, Y. Electroactive covalent organic frameworks/carbon nanotubes composites for electrochemical sensing, *ACS Appl. Nano Mater.* **2020**, *3*, 1412–1419.

35. Bai, Y.; Liu, Y.; Liu, M.; Wang, X.; Shang, S.; Gao, W.; Du, C.; Qiao, Y.; Chen, J.; Dong, J.; et al. Near-equilibrium growth of chemically stable covalent organic framework/graphene oxide hybrid materials for the hydrogen evolution reaction. *Angew. Chem. Int. Ed.* **2022**, *61*, 13067.
36. Sundaresan, R.; Mariyappan, V.; Chen, S.-M.; Alagarsamy, S.; Akilarasan, M. Fabrication of a new electrochemical sensor based on bimetal oxide for the detection of furazolidone in biological samples. *Micromachines* **2022**, *13*, 876. [CrossRef]
37. Wang, L.; Yang, Y.; Liang, H.; Wu, N.; Peng, X.; Wang, L.; Song, Y. A novel N, S-rich COF and its derived hollow N, S-doped carbon@Pd nanorods for electrochemical detection of Hg^{2+} and paracetamol. *J. Hazard. Mater.* **2021**, *409*, 124528. [CrossRef]
38. Liang, H.; Luo, Y.; Li, Y.; Song, Y.; Wang, L. An immunosensor using electroactive COF as signal probe for electrochemical detection of carcinoembryonic antigen. *Anal. Chem.* **2022**, *94*, 5352–5358. [CrossRef] [PubMed]
39. Sun, L.; Guo, H.; Pan, Z.; Liu, B.; Zhang, T.; Yang, M.; Wu, N.; Zhang, J.; Yang, F.; Yang, W. In-situ reducing platinum nanoparticles on covalent organic framework as a sensitive electrochemical sensor for simultaneous detection of catechol, hydroquinone and resorcinol. *Colloids Surf. A* **2022**, *635*, 128114. [CrossRef]
40. Huang, X.; Shi, W.; Li, J.; Bao, N.; Yu, C.; Gu, H. Determination of salivary uric acid by using poly(3,4-ethylenedioxythipohene) and graphene oxide in a disposable paper-based analytical device. *Anal. Chim. Acta* **2020**, *1103*, 75–83. [CrossRef]
41. Niu, X.; Bo, X.; Guo, L. MOF-derived hollow $NiCo_2O_4$/C composite for simultaneous electrochemical determination of furazolidone and chloramphenicol in milk and honey. *Food Chem.* **2021**, *364*, 130368. [CrossRef] [PubMed]
42. Gu, Q.; Wang, Z.; Qiao, L. Nitrogen-doped graphdiyne quantum dots for electrochemical chloramphenicol quantification in water. *ACS Appl. Nano Mater.* **2021**, *4*, 12755–12765. [CrossRef]
43. Shahrokhian, S.; Naderi, L.; Ghalkhani, M. Modified glassy carbon electrodes based on carbon nanostructures for ultrasensitive electrochemical determination of furazolidone. *Mater. Sci. Eng. C* **2016**, *61*, 842–850. [CrossRef] [PubMed]
44. Jaysiva, G.; Manavalan, S.; Chen, S. MoN nanorod/sulfur-doped graphitic carbon nitride for electrochemical determination of chloramphenicol. *ACS Sustain. Chem. Eng.* **2020**, *8*, 11088–11098. [CrossRef]
45. Melekhin, A.O.; Tolmacheva, V.V.; Shubina, E.G. Determination of nitrofuran metabolites in honey using a new derivatization reagent, magnetic solid−phase extraction and LC−MS/MS. *Talanta* **2021**, *230*, 122310. [CrossRef]
46. Piao, H.; Choi, G.; Jin, X.; Hwang, S.; Song, Y.; Cho, S.; Choy, J. Monolayer graphitic carbon nitride as metal-free catalyst with enhanced performance in photo- and electro-catalysis. *Nano-Micro Lett.* **2022**, *14*, 55. [CrossRef] [PubMed]
47. Veerakumar, P.; Sangili, A.; Chen, S.M. Fabrication of platinum−rhenium nanoparticles−decorated porous carbons: Voltammetric sensing of furazolidone. *ACS Sustain. Chem. Eng.* **2020**, *132*, 132210. [CrossRef]
48. Fotouhi, L.; Heravi, M.M. Heravi. Electrochemistry and voltammetric determination of furazolidone with a multi−walled nanotube composite film-glassy carbon electrode. *J. Appl. Electrochem.* **2011**, *41*, 137–142. [CrossRef]
49. Kdr, A.; Mgb, F.; Twcac, D. Porous-coral-like cerium doped tungsten oxide/graphene oxide micro balls: A robust electrochemical sensing platform for the detection of antibiotic residue. *Colloids Surf. A* **2021**, *628*, 127275.